

RSC Advances



This is an *Accepted Manuscript*, which has been through the Royal Society of Chemistry peer review process and has been accepted for publication.

Accepted Manuscripts are published online shortly after acceptance, before technical editing, formatting and proof reading. Using this free service, authors can make their results available to the community, in citable form, before we publish the edited article. This *Accepted Manuscript* will be replaced by the edited, formatted and paginated article as soon as this is available.

You can find more information about *Accepted Manuscripts* in the [Information for Authors](#).

Please note that technical editing may introduce minor changes to the text and/or graphics, which may alter content. The journal's standard [Terms & Conditions](#) and the [Ethical guidelines](#) still apply. In no event shall the Royal Society of Chemistry be held responsible for any errors or omissions in this *Accepted Manuscript* or any consequences arising from the use of any information it contains.



Journal Name

ARTICLE

Effects of microstructures on the compression behavior and phase transition routine of In_2O_3 nanocubes under high pressures

Shunxi Tang,^a Yan Li,^b Jian Zhang,*^a Hongyang Zhu,^a Yunxuan Dong,^a Pinwen Zhu*^a and Qiliang Cui^a

Received 00th January 20xx,
Accepted 00th January 20xx

DOI: 10.1039/x0xx00000x

www.rsc.org/

The differences between the compression behaviors of nanocrystal systems and their bulk counterparts are generally attributed to the size and morphology effects. However, these effects may not be simply employed to deal with the contradictory results about In_2O_3 bulk and nanomaterials under high pressures. In this work, we intend to show that other than size and morphology, the effects of microstructure should play a key role in the compression behavior and phase transition routine of In_2O_3 cubical-shaped nanocrystals under high pressures. Two samples of In_2O_3 nanocubes, which have almost the same size, shape and exposed facets, are subjected to high pressure at room temperature. The In_2O_3 nanocubes with a lower density of microstructures undergo a first order phase transition at about 18.9 GPa, and the two phases coexist when the pressure is released. Whereas the In_2O_3 nanocubes with a higher density of microstructures show no sign of such a phase transition at pressures up to 33.4 GPa, a change of elastic properties at about 8.8 GPa may be observed instead. Thus, it is anticipated that controlling the microstructures of nanomaterials may be a potential route to modulate their structural and elastic behaviors under pressures.

Introduction

High-pressure studies on nanostructured materials have attracted considerable scientific interest since nanocrystal systems exhibit novel compression behaviors different from those of their bulk counterparts.¹⁻⁷ Earlier studies have been focused on the size effect which has a strong influence on the critical pressures for phase transitions and the phase transition routines.¹⁻³ With the development of synthesis and preparation techniques, nanocrystals with controllable morphologies can be obtained. The effects of morphological features, such as shapes and exposed facets, on the structural behaviors of nanocrystal systems under high pressures, have attracted increasing research enthusiasm.⁴⁻⁷ Although the intrinsic nature that causes the differences in the compression behaviors of bulk and nanomaterials remains far from being fully discovered, the mechanism is generally attributed to nano-effects, such as the small size effect, surface and interface effect, etc., which are closely correlated with the large fraction of low-coordinated atoms at or near the surfaces of nanoscale materials¹⁻³. Yet another source of symmetry breaking atoms may be microstructures of crystals, such as lattice defects and microdomain boundaries. Especially the defect is one of the most important factors influencing the chemical and physical properties of materials and hence always a major concern⁸⁻¹⁰. The proportion of atoms related to

microstructures increases dramatically as the size of materials diminishes to the nanoscale. Thus in addition to size and morphology, the microstructures may be anticipated to play an important role in the compression behaviors of nanomaterials under high pressures. In this work, we intend to demonstrate the effects of microstructure on the compression behavior and phase transition routine of In_2O_3 cubical-shaped nanocrystals under high pressures.

As an important transparent conducting oxide, In_2O_3 has received substantial attention in a variety of technological applications, such as solar cells,^{11,12} light-emitting diodes,^{13,14} field-emission devices,¹⁵ liquid-crystal displays,¹⁶ and gas sensors.¹⁷⁻²⁰ The structures and properties of In_2O_3 under various temperature-pressure conditions have been the focus of intense research efforts. In_2O_3 crystallizes in a cubic bixbyite structure ($c\text{-In}_2\text{O}_3$, space group (SG) $Ia\bar{3}$, No. 206, $Z = 16$) at ambient conditions.²¹ Three metastable structures, namely the rhombohedral corundum-type phase ($\text{rh-In}_2\text{O}_3$, SG $R\bar{3}c$, No. 167, $Z = 6$), the orthorhombic $\text{Rh}_2\text{O}_3(\text{II})$ -type phase ($\text{o1-In}_2\text{O}_3$, SG $Pbcn$, No. 60, $Z = 4$), and the orthorhombic $\alpha\text{-Gd}_2\text{S}_3$ -type phase ($\text{o2-In}_2\text{O}_3$, SG $Pnma$, No. 62, $Z = 4$), have been known for years.²² Recently, the rhombohedral corundum-type structure of In_2O_3 has been synthesized at ambient conditions in a metastable way in different nanostructures and thin films.²³⁻²⁷ In particular, the corundum phase is expected to show better properties and performances than the bixbyite phase, such as higher stability and conductivity.^{28,29} Farvid et al. demonstrated that under ambient pressure and temperature of 523 K, when the diameter of nanocrystals (D) is smaller than 5 nm, $\text{rh-In}_2\text{O}_3$ phase is present, while $c\text{-In}_2\text{O}_3$ phase remains at $D > 5$ nm.³⁰ The effects of temperature and pressure on the

^a State Key Laboratory of Superhard Materials, Jilin University, Changchun, 130012, China. E-mail: zhang_jian@jlu.edu.cn, zhupw@jlu.edu.cn

^b College of physics, Jilin University, Changchun, 130012, China.

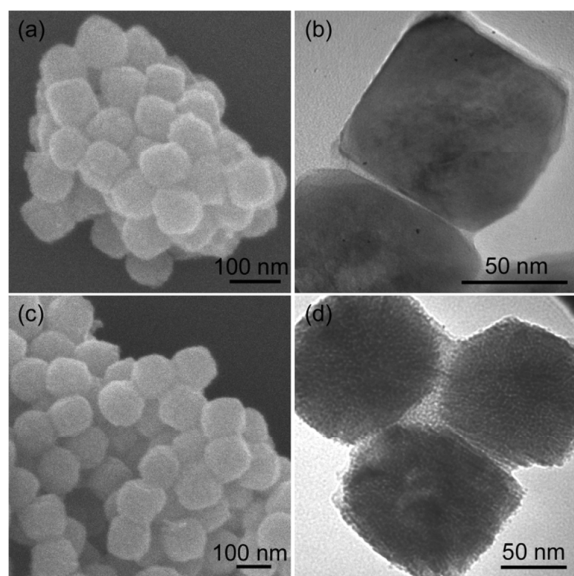


Fig. 1 (a,b) The SEM image and high-magnification TEM image of uniform c-In₂O₃ nanocubes (S1) synthesized at 210 °C with the heating rate of 4 °C/min. (c,d) The SEM image and high-magnification TEM image of uniform c-In₂O₃ nanocubes (S2) synthesized at 180 °C with the heating rate of 8 °C/min.

size-dependent solid phase transition of the In₂O₃ nanocrystals have been theoretically investigated on the basis of a simple thermodynamic model.³¹ It is demonstrated that the transition pressure and temperature changes are dominated by surface energy and surface stress.^{30,32} Therefore, it is of great interest to study the various pressure induced phases of In₂O₃. A few works about the high-pressure studies of In₂O₃ have been reported, yet contradictory results have been yielded. Liu *et al.* and Qi *et al.* found a phase transition from c-In₂O₃ to rh-In₂O₃ at the pressure range of 15 to 25 GPa in In₂O₃ bulk material and 6 nm nanoparticles.^{33,34} On the contrary, García-Domene *et al.* found no sign of such a phase transition under pressures up to 30 GPa, either in c-In₂O₃ bulk material or in 9 nm nanocrystals.³⁵ In a latest work by García-Domene *et al.*, c-In₂O₃ undergoes a transition to the Rh₂O₃(II) structure, instead of rh-In₂O₃, at about 35 GPa on the upstroke of pressure.³⁶ Moreover, on decreasing pressure, a previously unknown phase, the orthorhombic Rh₂O₃(III) phase (o3-In₂O₃, SG Pbcn, No.61, Z = 8), was found to occur at about 12 GPa. On further decreasing of pressure, a phase transition to the metastable corundum-type In₂O₃ was observed near room conditions. Apparently, these discrepancies cannot be explained simply by the size and morphology effects. The complicated phase transition sequence strongly implies there exists factors, other than size and morphology, that may have an important influence on the compression behaviors of In₂O₃ materials, especially in the nanoscale.

In this work, two kinds of In₂O₃ nanocubes, sample 1 (S1) and sample 2 (S2), were subjected to high pressure at room temperature. They have almost the same size (~100 nm), shape and exposed facets, as shown in Fig. 1a,b and c,d, respectively. In both of the two samples, each nanocube is

single crystalline. However, the microstructures should be different for the two samples, since they are prepared via different growth mechanisms. As described in our previous work,³⁷ S2 was grown via the self-assembly of uniform nanowires (2~3 nm in diameter). During the oriented attachment of the nanowires, lattice mismatches induced defects in a high density, mainly in the form of dislocations. On the other hand, S1 was grown via the ostwald-ripening mechanism, which resulted in a density of defects much lower than S2. This research on the effects of microstructure on the compression behaviors could be helpful for the understanding of phase transition mechanisms of In₂O₃ and other nanomaterials.

Experimental

The samples of In₂O₃ nanocubes were prepared following the solvothermal method described in our previous work.³⁷ In a typical reaction, 0.1 g of indium(III) chloride tetrahydrate (InCl₃·4H₂O, 99.99%) was dissolved in 5 mL of oleylamine (C18-content 80–90%, Acros). Then, 8 mL of ethanol was dropped in under ultrasonication. When a clear solution was formed, it was transferred into a Teflon-lined stainless steel autoclave. The samples, S1 and S2, were synthesized at 210 °C with the heating rate of 4 °C/min and at 180 °C with the heating rate of 8 °C/min, respectively. The autoclave was maintained at the desired temperature for 24 h and then allowed to cool naturally to room temperature. The white precipitates were separated by centrifugation at 3000 rpm for 20 min and washed repeatedly with absolute ethanol to remove the residues and/or impurities. The collected products were dried at 50 °C for 4 h before further characterization.

A HITACHI S4800 field emission scanning electron microscope (FESEM) working at 25.0 kV was used to characterize the morphology of the samples. The transmission electron microscopy (TEM), high-resolution transmission electron microscopy (HRTEM) micrographs and the selected area electron diffraction (SAED) patterns were taken to observe the morphology and structure of the samples via a JEM-2200FS transmission electron microscope with an accelerating voltage of 200 kV, which is equipped with an energy dispersive spectrometer (EDS). High-pressure experiments were conducted by using a symmetric diamond anvil cell (DAC) furnished with 400 μm culet diamonds. The T301 stainless steel gasket was preindented by the diamonds to an initial thickness of about 53 μm and then a center hole of 200 μm in diameter was drilled as the sample chamber. The samples with the liquid quasihydrostatic pressure-transmitting medium (methanol/ethanol = 4:1) were loaded into the sample chamber along with a tiny ruby chip for pressure measurements. The angle-dispersive XRD experiments of sample 1 and 2 were carried out with a wavelength of 0.485946 Å at Cornell High Energy Synchrotron Source (CHESS) and with a wavelength of 0.4112 Å at the National Synchrotron Light Source (NSLS), the Brookhaven National Laboratory (BNL), respectively. The XRD patterns were collected using a

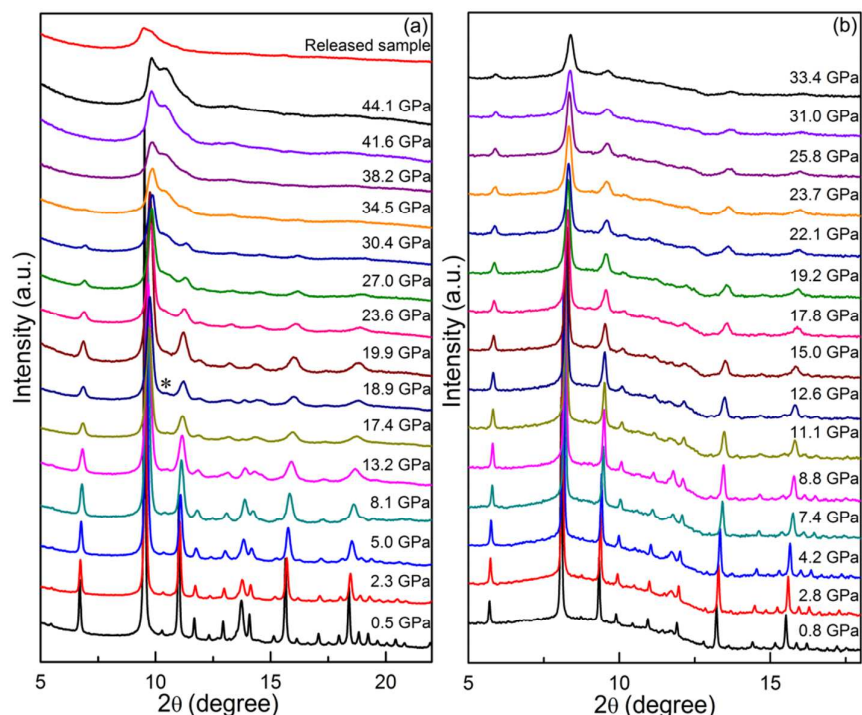


Fig. 2 (a) Angle dispersive XRD patterns of In_2O_3 nanocubes (S1) at elevated pressures at room temperature and released to ambient conditions. The asterisk indicates the appearance of a new broadened diffraction peak at 18.9 GPa. (b) Angle dispersive XRD patterns of In_2O_3 nanocubes (S2) at elevated pressures at room temperature.

Mar345

CCD detector and the one-dimensional diffraction profiles of intensity as a function of 2θ were obtained by integration of the observed two dimensional patterns with the Fit2D software.³⁸ Lattice parameters of the samples were obtained with Rietveld refinements of the powder XRD patterns performed using GSAS program packages.³⁹

Results and discussion

The *in situ* high pressure ADXRD patterns of sample 1 and 2 at pressures up to 44.1 and 33.4 GPa are shown in Fig. 2, respectively. It can be seen that all the diffraction peaks both in Fig. 2a and b shift to higher angles with increasing pressure due to the reduction of unit cell volume.

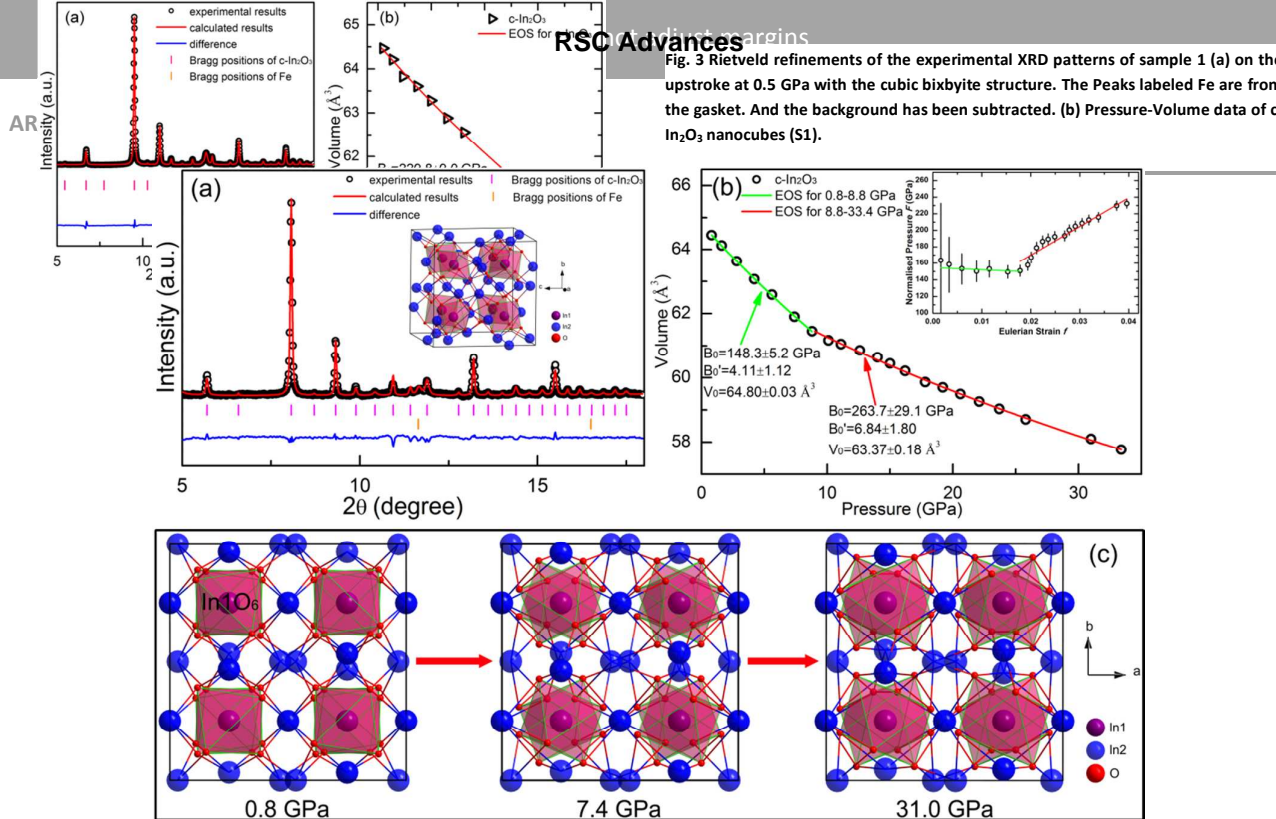


Fig. 3 Rietveld refinements of the experimental XRD patterns of sample 1 (a) on the upstroke at 0.5 GPa with the cubic bixbyite structure. The Peaks labeled Fe are from the gasket. And the background has been subtracted. (b) Pressure-Volume data of $c\text{-In}_2\text{O}_3$ nanocubes (S1).

As shown in Fig. 2a, at 0.5 GPa, all the diffraction peaks of S1 can be indexed to a cubic bixbyite phase (evidenced by the Rietveld refinement of the XRD pattern with $R_{wp} = 4.48\%$ shown in Fig. 3a). As the pressure is elevated, a new weak and broadened peak (marked with an asterisk) can be observed at 18.9 GPa, indicating the onset of a high-pressure phase transition. The broadening of the peak is likely due to the poor crystallinity under high pressures. From then on, the peaks of $c\text{-In}_2\text{O}_3$ and of the new phase coexist until it reached the highest pressure (~ 44.1 GPa) in this study. According to the only broadened peak, it is hardly possible to determine the structure of new phase. However, it should be noted that the value of transition pressure (~ 18.9 GPa) is much lower than the latest experimental value (~ 35 GPa) of García-Domene *et al.*,³⁶ who reported that bulk $c\text{-In}_2\text{O}_3$ undergoes a transition to the $\text{Rh}_2\text{O}_3(\text{II})$ structure. On the contrary, it is similar to the experimental values (15–25 GPa) of Liu *et al.* and Qi *et al.*,^{33,34} who have found a first order phase transition of In_2O_3 bulk and nano materials from cubic bixbyite to rhombohedral corundum structure under high pressures. Upon releasing pressure to ambient condition, both the diffraction peaks of the corundum phase and the new phase are retained, indicating that the high-pressure phase survive on release of pressure to ambient condition and that the phase transition is irreversible. These results also agree well with the reports of Liu *et al.* and Qi *et al.*^{33,34} Thus, it can be roughly speculated

that the new phase may quite possibly be $\text{rh-In}_2\text{O}_3$. However, the situation is quite different in the case of sample 2. As shown in Fig. 2b, at 0.8 GPa, all diffraction peaks can be indexed to the cubic bixbyite phase (evidenced by the Rietveld refinement of the XRD pattern with $R_{wp} = 1.69\%$ shown in Fig. 4a). With the increasing of the pressure, no sign of a phase transition can be observed in the whole upstroke until the pressure reaches 33.4 GPa.

The difference in the compression behaviour of S1 and S2 can also be visualized from the P-V plots. As shown in Figure 3b, fitted with the third-order Birch–Murnaghan equation of state, the derived parameters for $c\text{-In}_2\text{O}_3$ are $B_0 = 229.8 \pm 9.0$ GPa, $B_0' = 5.17$, $V_0 = 64.57 \text{ \AA}^3$ (where V_0 , B_0 and B_0' are the zero-pressure volume, bulk modulus, and pressure derivative of bulk modulus, respectively). The bulk moduli obtained in this study are higher than the reported values of In_2O_3 bulk materials,^{33,34,36,40,41} but smaller than those of the 6 nm In_2O_3 nanoparticles.^{33,34} Such a phenomenon, *i.e.*, the smaller the size, the higher the bulk modulus, is generally attributed to nano-size effect.

Contrary to the volume evolution of S1 as a function of pressure, there is a inflection at 8.8 GPa in the P–V plot of S2, as shown in Fig. 4b. The inset shows the plot of finite strain f against normalized stress F (f – F plot), which is useful to visualize slight anomalies of EOS that is difficult to find in the pressure–volume plot.^{42–44} Where the finite strain f and normalized stress F are defined as follows:

$$f = [(V_0/V)^{2/3} - 1]/2 \quad (1)$$

$$F = P/[3f(1 + 2f)^{5/2}] \quad (2)$$

The f - F plot shows almost horizontal variation before a inflection point corresponding to the pressure of 8.8 GPa and then changes to a positive slope. This agrees well with the P - V plot which indicate that there is also a change of the elastic property at 8.8 GPa. Thus two individual third-order Birch-Murnaghan EOSs were adopted, which are separated at the pressure (8.8 GPa) where the elastic property changes. As shown in Fig. 4b, in the range of 0.8–8.8 GPa, the derived parameters of c - In_2O_3 are $B_0 = 148.3 \pm 5.2$ GPa, $B_0' = 4.11$, $V_0 = 64.80 \text{ \AA}^3$ and in the range of 8.8–33.4 GPa, they are $B_0 = 263.7 \pm 29.1$ GPa, $B_0' = 6.84$, $V_0 = 63.37 \text{ \AA}^3$. Fig. 4c shows the evolution of the crystal structure of In_2O_3 nanocubes (S2) with increasing pressure, projecting along the c axis. It can be seen that, below 8.8 GPa, the neighboring $\text{In}1\text{O}_6$ octahedrons rotate reciprocally in the a - b plane as the pressure increases. It may be suggested that the lower bulk modulus at this pressure range may be due to reciprocal rotation of the neighboring $\text{In}1\text{O}_6$ octahedrons. Once the pressure is raised over 8.8 GPa, those $\text{In}1\text{O}_6$ octahedrons can be hardly rotated any more. The $\text{O}-\text{In}2$ bonds tend to be parallel to the a or b axis with increasing pressure. Thus, the material becomes less compressible and a higher bulk modulus is obtained as compared to its behavior at lower pressures.

In this study, the compression behavior of S1 bears much resemblance to those of In_2O_3 bulk material and 6 nm nanoparticles reported by Liu *et al.* and Qi *et al.*^{33,34} An irreversible phase transition is characteristic. Whereas the compression behavior of S2 is consistent with the reports by García-Domene *et al.*,³⁵ with no sign of a phase transition under pressures up to 33.4 GPa. Keeping in mind that S1 and S2 have almost the same size, shape, exposed surfaces and orientation, the difference in their compression behaviors cannot be simply explained by the size and morphology effects. As is mentioned above, the intrinsic difference between S1 and S2 lies in their different densities of microstructures. Thus microstructures should play a key role in the compression behaviors of In_2O_3 nanocubes, and have to be taken into account when other nanomaterials are subjected to high pressures. In addition, pressure-induced phase transition has become a powerful technique to obtain metastable materials with desirable properties and applications. Examples are abundant both in the literature and in industry, such as the syntheses of diamond and cubic boron nitride via HPHT techniques. Our work implies that the phase transition routine and the corresponding critical pressure may be modulated in a controllable way through careful design of the microstructure of materials in the nanoscale, and thus may be of keen interest in the relevant field.

Conclusions

In summary, the effects of microstructure on the compression and phase transition behaviours of In_2O_3 nanocubes were studied by using diamond anvil cell and *in situ* synchrotron X-ray powder diffraction technique at room temperature. A first order phase transition was observed to start at 18.9 GPa and remain far from being completed even at pressures of up to 44.1 GPa in the In_2O_3 nanocubes with a lower density of microstructures. The c - In_2O_3 and the undetermined high pressure phase coexisted when the pressure was released to ambient condition. Due to size effect, the bulk modulus of c - In_2O_3 is higher than the reported values of In_2O_3 bulk materials, but smaller than the 6 nm In_2O_3 nanoparticles. In contrast, not a phase transition but a change of the elastic properties at about 8.8 GPa was found in In_2O_3 nanocubes with a higher density of microstructures. Taking into account that the two samples have almost the same size, shape, exposed surfaces and orientation, this work strongly indicates that the microstructure is an important factor which may induce difference in the compression and phase transition behaviors of nanomaterials under high pressure.

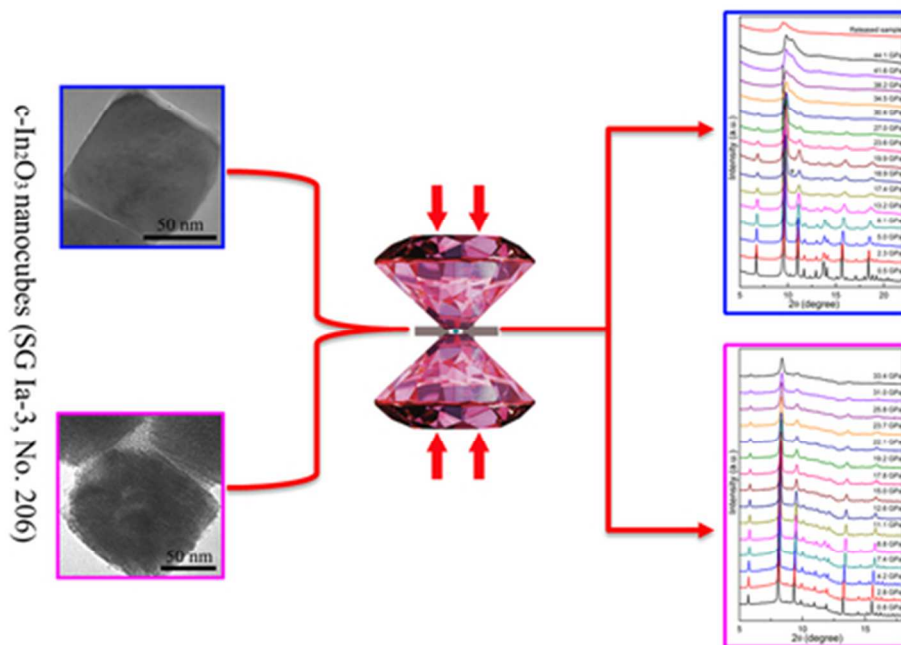
Acknowledgements

This work was supported in part by the National Natural Science Foundation of China (grant nos. 50772043, 51172087, and 11074089) and the National Basic Research Program of China (grant no. 2011CB808200).

Notes and references

- Z. W. Wang and Q. X. Guo, *J. Phys. Chem. C*, 2009, **113**, 4286–4295.
- Y. He, J. F. Liu, W. Chen, Y. Wang, H. Wang, Y. W. Zeng, G. Q. Zhang, L. N. Wang, J. Liu, T. D. Hu, H. Hahn, H. Gleiter and J. Z. Jiang, *Phys. Rev. B*, 2005, **72**, 212102.
- L. Wang, W. Yang, Y. Ding, Y. Ren, S. Xiao, B. Liu, S. V. Sinogeikin, Y. Meng, D. J. Gosztola, G. Shen, R. J. Hemley, W. L. Mao and H.-k. Mao, *Phys. Rev. Lett.*, 2010, **105**, 095701.
- S. -W. Park, J. -T. Jang, J. Cheon, H. -H. Lee, Lee, D. R. Lee, Y. Lee, Shape-Dependent Compressibility of TiO_2 Anatase Nanoparticles. *J. Phys. Chem. C*, 2008, **112**, 9627–9631.
- Z. W. Wang, L. L. Daemen, Y. S. Zhao, C. S. Zha, R. T. Downs, X. D. Wang, Z. L. Wang and R. J. Hemley, *Nature mater.*, 2005, **4**, 922–927.
- Y. J. Wang, J. Z. Zhang, J. Wu, J. L. Coffey, Z. J. Lin, S. V. Sinogeikin, W. G. Yang and Y. S. Zhao, *Nano. Lett.*, 2008, **8**, 2891–2895.
- B. Liu, M. G. Yao, B. B. Liu, Z. P. Li, R. Liu, Q. J. Li, D. M. Li, B. Zou, T. Cui and G. T. Zou, *J. Phys. Chem. C*, 2011, **115**, 4546–4551.
- Z. Q. Liu, D. P. Leusink, X. Wang, W. M. Lü, K. Gopinadhan, A. Annadi, Y. L. Zhao, X. H. Huang, S.W. Zeng, Z. Huang, A. Srivastava, S. Dhar, T. Venkatesan and Ariando, *Phys. Rev. Lett.*, 2011, **107**, 146802.

- 9 Z. Q. Liu, C. J. Li, W. M. Lü, X. H. Huang, Z. Huang, S.W. Zeng, X. P. Qiu, L. S. Huang, A. Annadi, J. S. Chen, J. M. D. Coey, T. Venkatesan and Ariando, *Phys. Rev. X*, 2013, **3**, 021010.
- 10 Z. Q. Liu, D. P. Leusink, W. M. Lü, X. Wang, X. P. Yang, K. Gopinadhan, Y. T. Lin, A. Annadi, Y. L. Zhao, A. Roy Barman, S. Dhar, Y. P. Feng, H. B. Su, G. Xiong, T. Venkatesan, and Ariando, *Phys. Rev. B*, 2011, **84**, 165106.
- 11 C. Y. Huang, G. C. Lin, Y. J. Wu, T. Y. Lin, Y. J. Yang and Y. F. Chen, *J. Phys. Chem. C*, 2011, **115**, 13083–13087.
- 12 T. P. Brennan, J. T. Tanskanen, K. E. Roelofs, J. W. F. To, W. H. Nguyen, J. R. Bakke, I. -K. Ding, B. E. Hardin, A. Sellinger, M. D. McGehee and S. F. Bent, *J. Phys. Chem. C*, 2013, **117**, 24138–24149.
- 13 H. Q. Cao, X. Q. Qiu, Y. Liang, Q. M. Zhu and M. J. Zhao, *Appl. Phys. Lett.*, 2003, **83**, 761–763.
- 14 L.-C. Chen, C.-H. Tien and W.-C. Liao, *J. Phys. D: Appl. Phys.* 2011, **44**, 165101.
- 15 J. Lin, Y. Huang, Y. Bando, C. C. Tang, C. Li and D. Golberg, *ACS Nano*, 2010, **4**, 2452–2458.
- 16 Hsu, S. F.; Lee, C. C.; Hwang, S. W.; Chen, C. H. Highly Efficient Top-Emitting White Organic Electroluminescent Devices. *Appl. Phys. Lett.* 2005, **86**, 253508.
- 17 X. L. Hu, X. Zhou, B. Wang, P. Sun, X. W. Li, C. Wang, J. Y. Liu and G. Y. Lu, *RSC Adv.*, 2015, **5**, 4609–4614.
- 18 M. Karmaoui, S. G. Leonardi, D. M. Tobaldi, N. Donato, R. C. Pullar, M. P. Seabra, J. A. Labrincha, and G. Neri, *J. Mater. Chem. B*, 2015, **3**, 399–407.
- 19 W. L. Zang, Y. X. Nie, D. Zhu, P. Deng, L. L. Xing and X. Y. Xue, *J. Phys. Chem. C*, 2014, **118**, 9209–9216.
- 20 C. H. Zhao, G. Z. Zhang, W. H. Han, J. C. Fu, Y. M. He, Z. X. Zhang, and E. Q. Xie, *CrystEngComm*, 2013, **15**, 6491–6497.
- 21 M. Marezio, *Acta Crystallogr.*, 1966, **20**, 723–728.
- 22 M. F. Bekheet, M. R. Schwarz, S. Lauterbach, H.-J. Kleebe, P. Kroll, R. Riedel and A. Gurlo, *Angew. Chem. Int. Ed.*, 2013, **52**, 6531–6535.
- 23 A. Gurlo, N. Barsan, U. Weimar, M. Ivanovskaya, A. Taurino, and P. Siciliano, *Chem. Mater.*, 2003, **15**, 4377–4383.
- 24 D. Yu, S.-H. Yu, S. Zhang, J. Zuo, D. Wang, and Y. T. Qian, *Adv. Funct. Mater.*, 2003, **13**, 497–501.
- 25 M. Epifani, P. Siciliano, A. Gurlo, N. Barsan, and U. Weimar, *J. Am. Chem. Soc.*, 2004, **126**, 4078–4079.
- 26 J. Q. Xu, Y. P. Chen, Q. Y. Pan, Q. Xiang, Z. X. Cheng, and X. W. Dong, *Nanotechnology*, 2007, **18**, 115615.
- 27 Z. Zhuang, Q. Peng, J. Liu, X. Wang, and Y. Li, *Inorg. Chem.*, 2007, **46**, 5179–5187.
- 28 S. Zh Karazhanov, P. Ravindran, P. Vajeeston, A. Ulyashin, T. G. Finstad, and H. Fjellvag, *Phys. Rev. B*, 2007, **76**, 075129.
- 29 A. Gurlo, M. Ivanovskaya, N. Barsan, and U. Weimar, *Inorg. Chem. Commun.*, 2003, **6**, 569–572.
- 30 S. S. Farvid, N. Dave and P. V. Radovanovic, *Chem. Mater.*, 2010, **22**, 9–11.
- 31 X. B. Jiang, M. Jiang and M. Zhao, *Chem. Phys. Lett.*, 2013, **563**, 76–79.
- 32 A. Gurlo, *Angew. Chem. Int. Ed.*, 2010, **49**, 5610–5612.
- 33 D. Liu, W. W. Lei, B. Zou, S. D. Yu, J. Hao, K. Wang, B. B. Liu, Q. L. Cui and G. T. Zou, *J. Appl. Phys.*, 2008, **104**, 083506.
- 34 J. Qi, J. F. Liu, Y. He, W. Chen and C. Wang, *J. Appl. Phys.*, 2011, **109**, 063520.
- 35 B. García-Domene, H. M. Ortiz, O. Gomis, J. A. Sans, F. J. Manjón, A. Muñoz, P. Rodríguez-Hernández, S. N. Achary, D. Errandonea, D. Martínez-García, A. H. Romero, A. Singhal and A. K. Tyagi, *J. Appl. Phys.*, 2012, **112**, 123511.
- 36 B. García-Domene, J. A. Sans, O. Gomis, F. J. Manjón, H. M. Ortiz, D. Errandonea, D. Martínez-García, R. Vilaplana, A. L. J. Pereira, A. Morales-García, P. Rodríguez-Hernández, A. Muñoz, C. Popescu and A. Segura, *J. Phys. Chem. C*, 2014, **118**, 20545–20552.
- 37 S. X. Tang, J. Zhang, S. Wu, C. Y. Hu, Y. A. Li, L. N. Jiang and Q. L. Cui, *J. Phys. Chem. C*, 2014, **118**, 21170–21176.
- 38 A. P. Hammersley, S. O. Svensson, M. Hanfland, A. N. Fitch and D. Hausermann, *High Press. Res.*, 1996, **14**, 235–248.
- 39 B. H. Toby, *J. Appl. Crystallogr.*, 2001, **34**, 210–213.
- 40 C. T. Prewitt, R. D. Shannon, D. B. Rogers and A. W. Sleight, *Inorg. Chem.*, 1969, **8**, 1985–1993.
- 41 H. Yusa, T. Tsuchiya, N. Sata and Y. Ohishi, *Phys. Rev. B*, 2008, **77**, 064107.
- 42 R. J. Angel, *Rev. Mineral Geochem.*, 2000, **41**, 35–59.
- 43 A. Sano-Furukawa, T. Yagi, T. Okada, H. Gotou and T. Kikegawa, *Phys. Chem. Miner.*, 2012, **39**, 375–383.
- 44 J. Darul, C. Lathe and P. Piszora, *J. Phys. Chem. C*, 2013, **117**, 23487–23494.



In addition to size and morphology, the microstructure may play an important role and induce differences in the compression and phase transition behaviors of nanomaterials under high pressures.
39x28mm (300 x 300 DPI)